Bimodal regulation of ICR1 levels generates self-organizing auxin distribution

Ora Hazak[a], Uri Obolski[a], Tomáš Prat[b], Jiří Friml[b], Lilach Hadany[a], and Shaul Yalovsky[a,1]

[a]Department of Molecular Biology and Ecology of Plants, Tel Aviv University, Tel Aviv 69978, Israel; and [b]Institute of Science and Technology (IST Austria), A–3400 Klosterneuburg, Austria

Edited by Mark Estelle, University of California, San Diego, La Jolla, CA, and approved November 11, 2014 (received for review July 22, 2014)

Auxin polar transport, local maxima, and gradients have become an important model system for studying self-organization. Auxin distribution is regulated by auxin-dependent positive feedback loops that are not well-understood at the molecular level. Previously, we showed the involvement of the RHO of Plants (ROP) effector INTERACTOR of CONSTITUTIVELY active ROP 1 (ICR1) in regulation of auxin transport and that ICR1 levels are posttranscriptionally repressed at the site of maximum auxin accumulation at the root tip. Here, we show that bimodal regulation of ICR1 levels by auxin is essential for regulating formation of auxin local maxima and gradients. ICR1 levels increase concomitant with increase in auxin response in lateral root primordia, cotyledon tips, and provascular tissues. However, in the embryo hypophysis and root meristem, when auxin exceeds critical levels, ICR1 is rapidly destabilized by an $SCF^{(TIR1/AFB)}$ [SKP, Cullin, F-box (transport inhibitor response 1/auxin signaling F-box protein)]-dependent auxin signaling mechanism. Furthermore, ectopic expression of ICR1 in the embryo hypophysis resulted in reduction of auxin accumulation and concomitant root growth arrest. ICR1 disappeared during root regeneration and lateral root initiation concomitantly with the formation of a local auxin maximum in response to external auxin treatments and transiently after gravitropic stimulation. Destabilization of ICR1 was impaired after inhibition of auxin transport and signaling, proteasome function, and protein synthesis. A mathematical model based on these findings shows that an in vivo-like auxin distribution, rootward auxin flux, and shootward reflux can be simulated without assuming preexisting tissue polarity. Our experimental results and mathematical modeling indicate that regulation of auxin distribution is tightly associated with auxin-dependent ICR1 levels.

auxin | transport | pattern formation | ROP GTPases | root development

The distribution of auxin in plants has become an important model system for studying the links between cell polarity and pattern formation. Polar auxin transport, maxima, and gradients regulate the initiation, positioning, shape, and size of new organs (1–9). Auxin is synthesized in different parts of the plant, primarily in young leaves (10, 11), from where it is transported to the root and a local auxin maximum is formed close to the root tip (2). Directional auxin transport depends on polar membrane localization of PIN auxin efflux transporters (12, 13), their activating AGCVIII kinases (group VIII of plant serine/threonine protein kinases related to mammalian protein kinase A, cyclic GMP related protein kinases and protein kinase C group VIII) (14–16), and close to the root tip, the auxin influx transporter AUX1 as well (17).

It has been suggested that the formation of local auxin maxima in the root depends on polar PIN localization (6), local auxin synthesis at the root tip (18), and a combination of AUX1/Like AUX1 auxin influx, which determine cellular auxin levels and PIN-dependent directional auxin efflux (19). It is not known yet how auxin levels are interpreted to regulate PIN polarization. Earlier work and modeling that became known as the "canalization hypothesis" suggested that auxin enhances its own flux by a positive feedback loop, resulting in auxin transporting cell files that, in turn, differentiate into vascular tissues (8, 20–24).

An example of an auxin-modulated feedback loop, which regulates directional auxin transport, was found in the *Arabidopsis* shoot apical meristem. The MACCHI-BOU 4/NONPHOTOTROPIC HYPOCOTYL 3-like family proteins function redundantly in regulation of PIN1 polarity. Auxin induces MACCHI-BOU 4 expression, which in turn, induces rootward PIN1 polarization at the site of auxin maximum formation in the L1 layer. The rootward PIN1 localization is required for auxin transport away from the meristem (25). However, it is not known whether similar auxin-modulated feedback loops exist in other tissues, and the molecular mechanisms that could explain the canalization hypothesis are not well-understood (8).

Previously, we identified the RHO of Plants (ROP) effector INTERACTOR of CONSTITUTIVELY active ROP 1 (ICR1) and showed that it is required for recruitment of PIN proteins to the plasma membrane (26, 27). ICR1 expression is induced by auxin, and it is posttranscriptionally repressed at the site of auxin maximum formation at the root tip (26). Here, using experimental work and modeling, we show that cellular auxin levels regulate ICR1 stability and that this mechanism can support polar auxin transport and local maxima formation.

Results and Discussion

Ectopic Expression of ICR1 in the Hypophysis. GFP-ICR1 (which can complement the *icr1* root phenotype) (26) was not detected at the site of auxin accumulation in the embryo hypophysis [the embryonic cell from which the quiescent center (QC) and the root cap develop], the root QC, or neighboring initial cells (26) (Fig. 1 *A* and *B* and Fig. S1*A*). Even when overexpressed under regulation of the constitutive *35S* promoter, GFP-ICR1 or the ICR1 promoter (*pICR1*) -driven ICR1-mCherry was still undetectable in

Significance

In nature, patterns form by self-organizing mechanisms that involve distribution of components called morphogens. In many cases, the molecular mechanisms that underlie morphogen distribution in living organisms are not well-known. In plants, a small molecule called auxin serves as a morphogen that regulates diverse developmental processes. The ability of cells to transport or accumulate auxin defines its distribution. Here, we present experimental data and theoretical modeling showing that auxin concentrations regulate the levels of a protein called INTERACTOR of CONSTITUTIVELY active ROP (RHO of Plants) 1 (ICR1), which is required for auxin transport. ICR1 expression is induced by auxin, but when auxin levels exceed a critical concentration, ICR1 is rapidly degraded, leading to auxin accumulation. Thus, auxin self-regulates its distribution by bimodal regulation of ICR1.

Author contributions: L.H. and S.Y. designed research; O.H., U.O., and T.P. performed research; O.H., J.F., L.H., and S.Y. analyzed data; and O.H., U.O., J.F., L.H., and S.Y. wrote the paper.

The authors declare no conflict of interest.

This article is a PNAS Direct Submission.

[1]To whom correspondence should be addressed. Email: shauly@tauex.tau.ac.il.

This article contains supporting information online at www.pnas.org/lookup/suppl/doi:10.1073/pnas.1413918111/-/DCSupplemental.

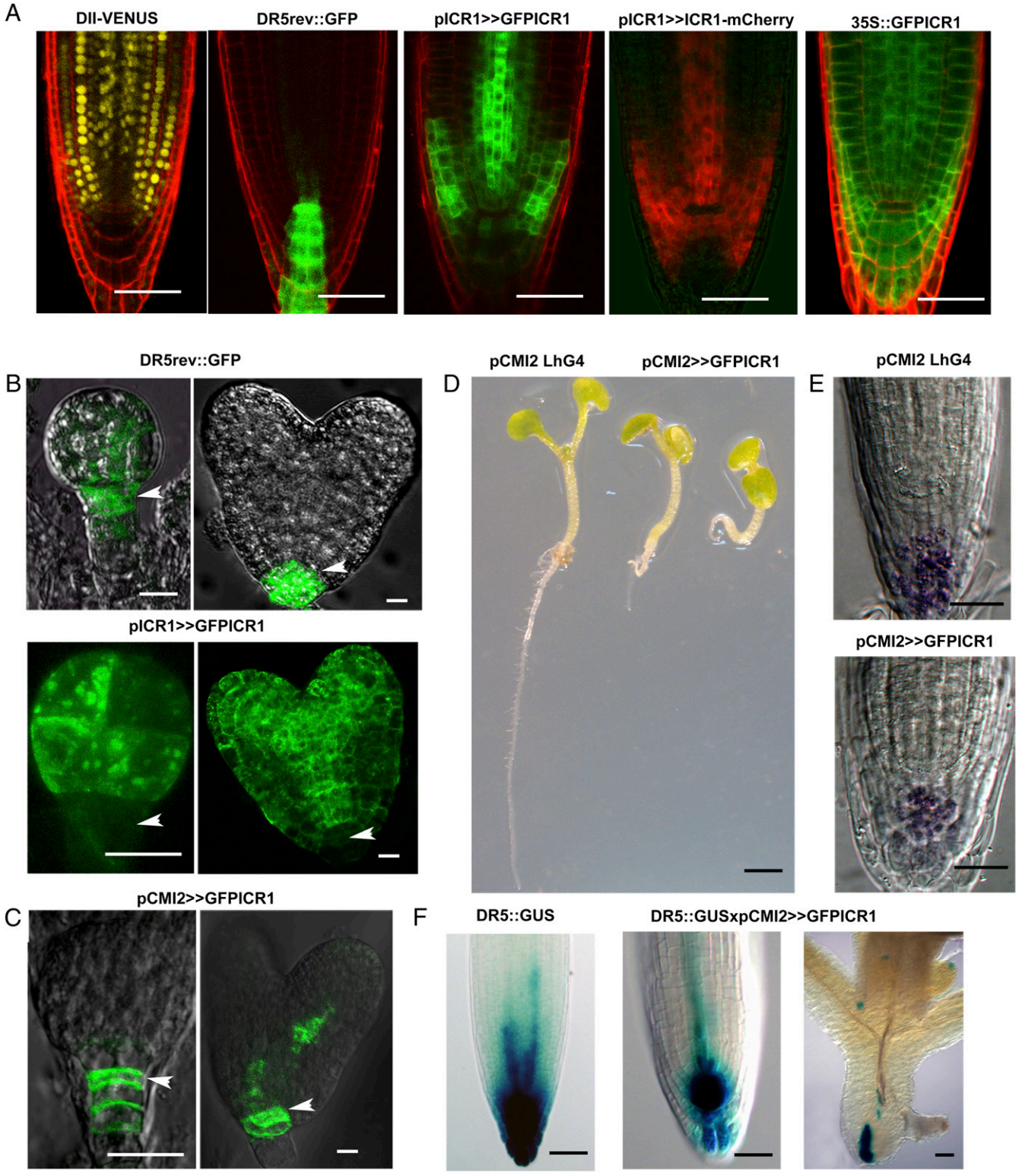

Fig. 1. ICR1 stability and auxin maximum formation. (*A*) ICR1 is down-regulated at the sites of auxin accumulation (DII-VENUS and $DR5_{rev}$::GFP) in the root QC. Down-regulation is seen with either GFP-ICR1 or ICR1-mCherry expressed from either the *ICR1* or *35S* promoter. (*B*) GFP-ICR1 (arrowheads) is absent from the site of auxin maximum formation ($DR5_{rev}$::GFP) in the embryo hypophysis of (*Left*) globular- and (*Right*) heart-stage embryos. (*C*) Ectopic expression of GFP-ICR1 from the *pCMI2* (pCMI2>>GFPICR1). Arrowheads denote expression of GFP-ICR1 in the hypophysis in (*Left*) globular- and (*Right*) heart-stage embryos. (*D*, *Left*) A control *pCMI2>>LhG4* plant with normally developed primary root and (*Center* and *Right*) two *pCMI2>>GFPICR1* plants with short primary roots. (*E*) Lugol staining showing reduced columella cell layers in *pCMI2>>GFPICR1* plants. (*F*) *DR5*::β-Glucoronidase (GUS) expression in (*Left*) *pCMI2>>LhG4* and (*Center* and *Right*) *pCMI2>>GFPICR1* backgrounds. (Scale bars: *A*, *E*, and *F*, 50 μm; *B* and *C*, 20 μm; *D*, 2 mm.)

the QC (Fig. 1*A*). Importantly, immunostaining with anti-ICR1 antibodies showed similar down-regulation of ICR1 at the root tip (Fig. S1*B*), indicating that the expression pattern of GFP-ICR1 reflects that of the native protein.

In parallel studies, we identified a gene designated *Ca^{2+} MODULATOR of ICR1 2* (*CMI2*), in which expression can already be detected in the suspensor of the globular embryo and later, in the hypophysis and QC cells (Fig. 1*C*) before generation of a stable auxin maximum. We expressed GFP-ICR1 under the regulation of the *CMI2* promoter (*pCMI2*) to examine if and how ectopic expression of ICR1 would affect meristem maintenance and auxin maximum formation. Expression of GFP-ICR1 under regulation of the *pCMI2* (Fig. 1*D*, pCMI2>>GFPICR1) using a transcription/transactivation system (26, 28) resulted in a root growth arrest (Fig. 1 *D–F*) that was associated with a collapse of the root apical meristem as detected by reduced columella layers (Fig. 1*E*) and a reduction in the auxin response at the root tip (Fig. 1*F*). The transactivation effect often results in high expression levels (29). Furthermore, microarray experiments (30) indicated that *CMI2* is an auxin-induced gene. Hence, the cumulative effect of the highly specific hypophysis and QC expression together with the transcription/transactivation and auxin induction resulted in high levels of GFP-ICR1 ectopic expression.

The auxin maximum in the root stem cell niche results from the action of PIN4 aided by other PIN auxin transporters (31). Thus, we tested whether PIN4 expression and subcellular localization were affected in *pCMI2>>GFP-ICR1* plants. Immunostaining with anti-PIN4 antibodies showed that PIN4 levels at the plasma membrane of the root meristem cells were lower and that the intracellular signal increased in *pCMI2>>GFP-ICR1* relative to levels and signal in control *pCMI2>>LhG4* (LhG4, a chimeric transcription factor comprising transcription transactivation domain II of *Saccharomyces cervisiae* GAL4 fused to mutant lac repressor) roots (Fig. S1 *C–F* and Table S1). This effect led to a less pronounced polarity of PIN4 localization as observed in provascular cells (Fig. S1 *D*, arrowheads, *E*, and *F*). Thus, the ectopic expression of ICR1 in the central root meristem impaired both the local auxin response maximum and the related auxin transport machinery. Because the PIN expression and PIN polar localization are feedback-regulated by auxin levels (23, 32, 33), these effects can mutually enhance each other, leading to the observed root meristem collapse.

Taken together, the data presented in Fig. 1 and Fig. S1 indicate that expression of ICR1 in the hypophysis impairs auxin accumulation and leads to root meristem collapse.

De Novo Auxin Accumulation and Exogenous Auxin Treatments Induce ICR1 Destabilization. To reveal whether the destabilization of ICR1 takes place before, concomitant with, or after formation of the auxin maximum at the root tip, we followed the changes in ICR1 levels during root regeneration and lateral root (LR) formation. It has been shown that, when sectioned at positions ≤200 μm from their tip, roots regenerated an apical meristem, whereas roots sectioned at positions ≥270 μm did not (34). We took advantage of this system and examined the persistence of GFP-ICR1 relative to the formation of the auxin maximum, which was detected with the auxin sensor DII-VENUS (35) (Fig. 2 *A* and *B* and Fig. S2 *A* and *B*). When roots were sectioned 170 μm from the tip, GFP-ICR1 was destabilized at the site of excision. However, when roots were sectioned 300 μm from the tip, the GFP-ICR1 signal did not decay, even after 48 h, and instead, an increased GFP-ICR1 signal was detected in more shootward positions that corresponded to dividing pericycle cells about to form a new LR (Fig. S2*B*).

We examined changes in DII-VENUS and GFP-ICR1 shortly after the root tip excision. Already after 30 min, the DII-VENUS signal was reduced by 40% adjacent to the site of root excision (Fig. 2*A*, arrowheads and Fig. S2 *C* and *D*), and at the same time, GFP-ICR1 was observed in subcellular compartments that resembled lytic vacuoles (Fig. 2*B*, arrowheads). After 1 h, the DII-VENUS signal was reduced by 60% (Fig. S2*D*), and the number of observed GFP-ICR1–containing compartments increased (Fig. 2*B*). Later, after 12 and 24 h, the DII-VENUS and GFP-ICR1 signals continued to decrease, and a new auxin maximum was created just above the site of root excision (Fig. 2 *A* and *B* and Fig. S2 *C* and *D*). The reduction in the DII-VENUS signal was verified by curve fitting: ratio = $1.123 - 0.126 \times \log(\text{time})$ ($R^2 = 0.83$, $P \leq 10^{-5}$).

To estimate the auxin concentration range at which GFP-ICR1 decayed, we treated roots expressing DII-VENUS with 10 nM, 100 nM, and 1 μM natural auxin indole 3-acetic acid (IAA), which was similar to the experimental system described by Band et al. (36). The initiation of GFP-ICR1 decay as observed by its accumulation in intracellular compartments was detected within 30 min. The DII-VENUS signal decayed ∼15 and 45 min after treatments with 1 μM and 100 nM IAA, respectively (Fig. 2*G*). Based on comparison with the reduction in DII-VENUS during root meristem regeneration, we estimate that the onset of GFP-ICR1 decay in sectioned root tips occurred when cellular auxin levels exceeded critical levels, resembling auxin concentrations in root epidermal and cortex cells treated with 100 nM IAA.

To examine whether treatments with exogenous auxin could induce the decay of GFP-ICR1 in not only root meristematic cells, roots were treated with 0.5 μM synthetic auxin analog naphthalene acetic acid (NAA) or 1 μM 2,4-dichlorophenoxyacetic acid (2,4-D), an auxin analog for which the AUX1-assisted influx into cells is highly efficient, but efflux is less efficient than that for IAA or NAA (37–39). After 3 h in NAA or 2,4-D, weak signal of the auxin response sensor $DR5_{rev}$::GFP (5) started to appear in the stele and the epidermis ∼500 μm shootward from the tip, concomitant with reduction in the GFP-ICR1 signal (Fig. 2*C* and Fig. S3). After 24 h, the GFP-ICR1 signal decayed completely at ∼500 μm shootward from the tip, while remaining less affected closer to the meristem (Fig. 2*C*, 24 h and Fig. S3). The DII-VENUS signal completely disappeared after 1 h in NAA or 2,4-D and reappeared closer to the root tip after 24 h. After treatments with 0.5 μM NAA, there was a 15-fold increase and a 3-fold decrease in the *DR5rev*::GFP GFP-ICR1 signals (Fig. S3 *B* and *C*). After 24 h in NAA, the $DR5_{rev}$::GFP signal increased by 110-fold, whereas the GFP-ICR1 decreased by 10-fold (Fig. S3 *B* and *C*). Statistical analysis confirmed that the differences between each time point were significant ($P \leq 0.0022$, Wilcoxon rank test). Hence, the decay of GFP-ICR1 was correlated with cellular auxin levels and not restricted to the meristem.

The persistence of the GFP-ICR1 signal after treatments with 10 nM, 100 nM, and 1 μM IAA was negatively correlated with auxin concentrations (Fig. 2 *D–F*). Similar to regenerating root meristem, GFP-ICR1 appeared in lytic vacuole-like compartments after 4 h of incubation in 10 μM IAA (Fig. 2*D*). However, GFP-ICR1 expression in the LR cap was not affected by exogenous auxin treatments, implying that ICR1 sensitivity to auxin-dependent destabilization is tissue-specific. Importantly, the data show that the natural auxin IAA (Fig. 2 *D–F*) and the synthetic auxin analogs NAA and 2,4-D (Fig. 2*C* and Fig. S3) induced similar decay of GFP-ICR1. Taken together, the results shown in Fig. 2 and Fig. S3 indicate that the destabilization of ICR1 depends on auxin concentration and can take place in the primary root meristem, stele, and to a lesser extent, LR cap. Furthermore, the treatments with exogenous auxins exemplified the bimodal nature of the regulation of ICR1 levels by auxin. On one hand, the 2,4-D and NAA treatments induced GFP-ICR1 expression in dividing pericycle cells and LR initiation sites that became sinks for auxin (Fig. 2*C*, 24 h and Fig. S3 *A* and *B*, 24 h). On the other hand, after accumulation of auxin in the tissue, GFP-ICR1 decayed (Fig. 2*C* and Fig. S3 *A–E*).

Dynamic Changes of ICR1 Levels During LR Development. LRs initiate from the pericycle at positions of localized auxin accumulation, and the formation and maintenance of their apical meristem

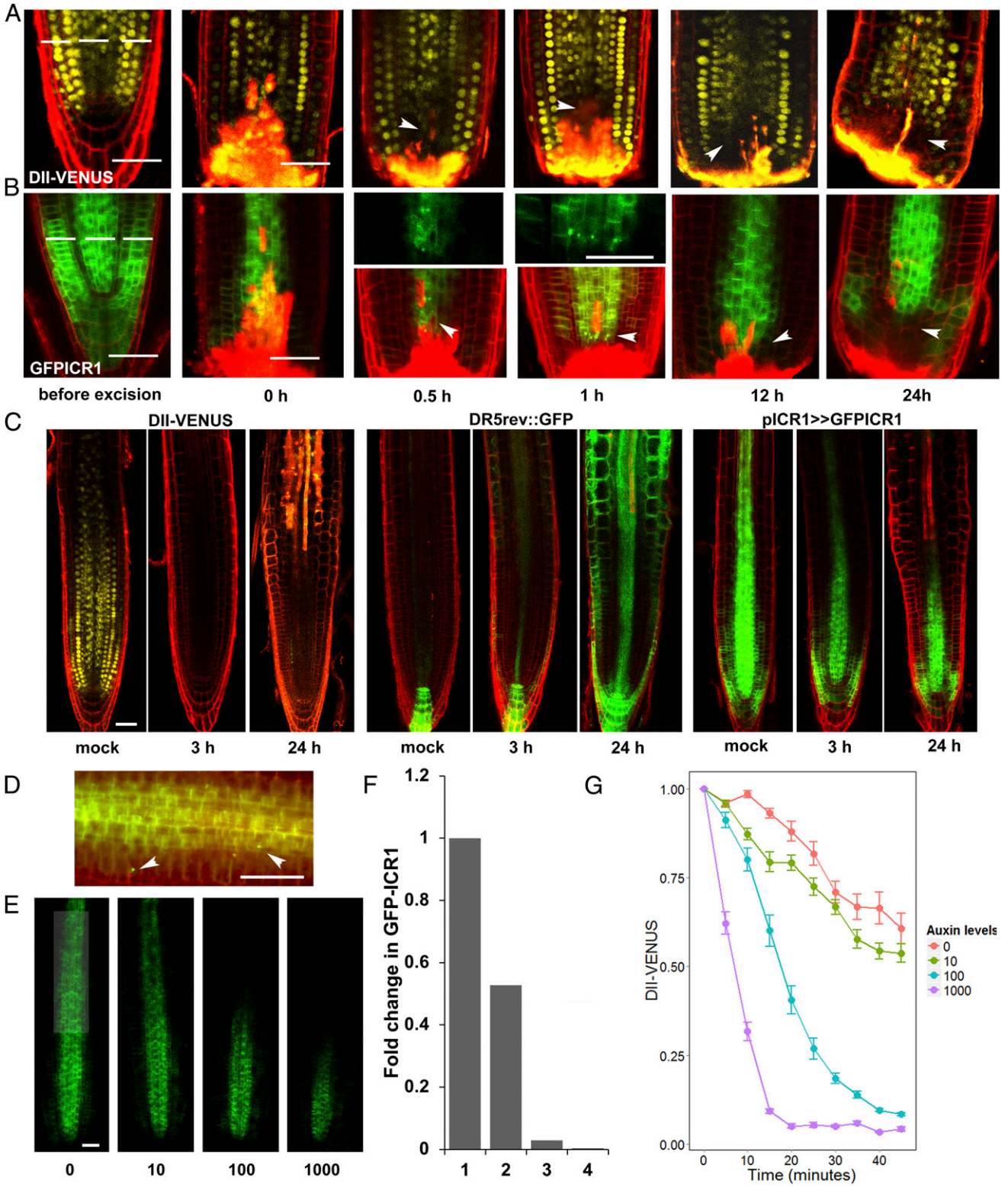

Fig. 2. High auxin concentrations initiate rapid GFP-ICR1 decay. Roots expressing (*A*) DII-VENUS or (*B*) GFP-ICR1 were sectioned 170 μm from the tip (dashed line). After 30 min, GFP-ICR1 started to appear in intracellular compartments and then disappeared concomitant with reduction in the DII-VENUS signal. Arrowheads denote (*A*) reduced DII-VENUS fluorescence and (*B*) intracellular GFP-ICR1 compartments and reduced fluorescence. (*C*) Incubation in 0.5 μM NAA led to rapid decay of the DII-VENUS signal, induction of $DR5_{rev}$::GFP, and decay of GFP-ICR1 500 μm from the root tip. (*D*) GFP-ICR1 was detected in intracellular compartments ~500 μm above the root tip after 4 h of incubation with 10 μM IAA (arrowheads). (*E*) Dose-dependent destabilization of GFP-ICR1 in seedlings incubated for 20 h in increasing concentrations of IAA (0–1,000 nM). (*F*) Quantification of the GFP-ICR1 signal shown in *E*. (*G*) DII-VENUS signal decreased after incubation of seedlings in increasing IAA concentrations (in nanomolar). Error bars are SE. (Scale bars: 50 μm.)

depend on a tip-localized auxin maximum and gradient (4, 40, 41). GFP-ICR1 expression was detected in LR founder cells and developing LR primordia (26) (Fig. 3 *F–J* and Fig. S4*A*). We followed the expressions of $DR5_{rev}$::GFP, *pICR1*>>GFP-ICR1, and the QC marker *pWOX5*::GFP_{ER} [ER localized GFP driven by the WUSHEL related homeobox 5 (WOX5) promoter] (42) during LR development. The developmental stages of the LRs were determined according to the work by Malamy and Benfey (41). Similar to the results with regenerating root apical meristems, the GFP-ICR1 signal started to decay concomitantly with the formation of a local auxin maximum at the LR tip in stage VI/emerging LR initials (LRIs) (Fig. 3 *B* and *G*, asterisks and Fig. S4 *A* and *B*). Quantification of the GFP-ICR1 signal showed that it was 20–25% weaker in stage VI/emerging LRIs compared with stages III and V LRIs (Fig. S4 *B* and *C*), and statistical analysis confirmed that the differences between the developmental stages were significant ($P \leq 0.002$, Wilcoxon rank test). The analysis of GFP-ICR1 expression in developing LRs showed that ICR1 expression is induced by auxin and destabilized when auxin levels increase. Notably, in developing LRs, expression of the QC marker *WOX5* starts in the LR founder cells in the pericycle before the establishment of an LR apical meristem or the formation of the auxin maximum (Fig. 3*K*). In contrast, ICR1 destabilization occurs during LR meristem maturation and might mark a new fully differentiated organizing center. Hence, auxin accumulation and ICR1 destabilization may occur in cells that have already begun to differentiate as part of the QC. The differential ability of cells to accumulate auxin and degrade ICR1 is in line with gene expression studies that showed that meristem regeneration competence is associated with specific gene expression profiles (34). In the primary root, the competence to accumulate auxin and degrade ICR1 is likely set in early embryogenesis, when the QC is defined (43, 44).

Decay of ICR1 Depends on Auxin Transport and Signaling. To obtain additional insight into the causal relationship between auxin accumulation and GFP-ICR1 decay, we performed a series of experiments with the auxin transport inhibitor *N*-1-naphtylphthalamic acid (NPA). Inhibition of auxin accumulation in sectioned root tips was observed after 3 h of incubation in NPA (Fig. 4*A*, DII-VENUS and $DR5_{rev}$::GFP in the +NPA 3 h column). Concomitantly, no decay of GFP-ICR1 was observed (Fig. 4*A*, GFPICR1 in the +NPA 3 h column). After prolonged incubation with NPA for 24 h, locally synthesized auxin accumulated at the root tip (45). Concomitantly with auxin accumulation, the GFP-ICR1 signal decayed and was not detectable in the sectioned root tips (Fig. 4*A*, GPFICR1 in the +NPA 24 h column).

To examine whether auxin signaling regulates ICR1 stability, root tips were sectioned 170 μm from the tip and then incubated with 5 μM $SCF^{(TIR1/AFB)}$ [SKP, Cullin, F-box (transport inhibitor response 1/auxin signaling F-box protein)] inhibitor auxinole (46, 47). After 5 h of incubation, the DII-VENUS signal increased rather than decayed, confirming inhibition of TIR1/AFB function (Fig. 4*B*, DII-VENUS in the auxinole 5 h column). The decay of the GFP-ICR1 signal was also inhibited by auxinole (Fig. 4*B*, GFPICR1 in the auxinole 5 h column), indicating that $SCF^{(TIR1/AFB)}$-dependent auxin signaling regulates ICR1 stability.

The $SCF^{(TIR1/AFB)}$-dependent decay of GFP-ICR1 could have been caused by a direct action of TIR1/AFB on GFP-ICR1 or TIR1/AFB-dependent gene expression. To distinguish between these two options, root tips were sectioned, and seedlings were

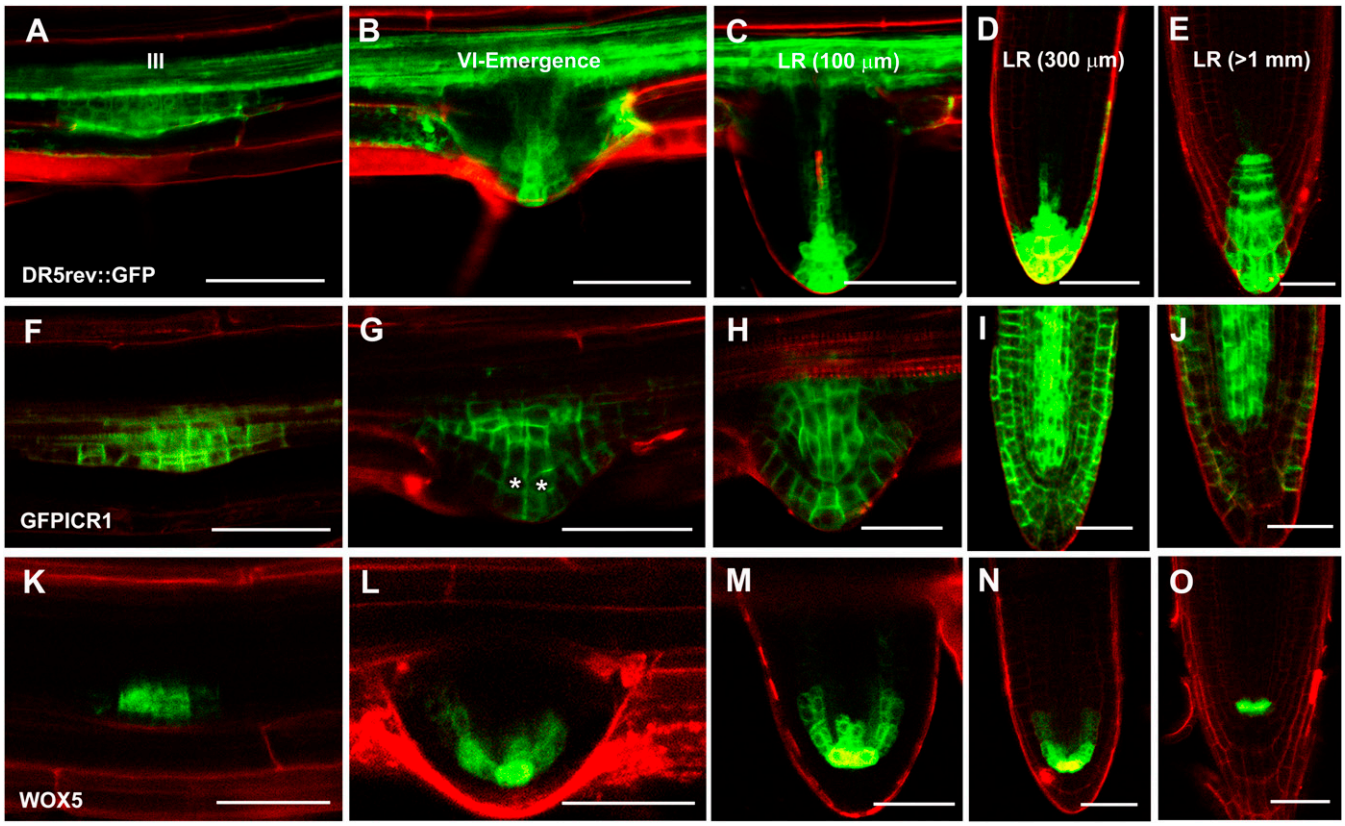

Fig. 3. Decay of GFP-ICR1 in developing LRs. (*A–E*) The auxin response marker $DR5_{rev}$::GFP, (*F–J*) GFP-ICR1, and (*K–O*) the QC marker *pWOX5*::GFP_{ER} during LR development starting from stage III (the LR developmental stages noted in *A–E* correspond to *F–O* as well). Note that changes in GFP-ICR1 levels correspond to auxin accumulation at the root tip. Asterisks in *G* highlight the cells with reduced GFP-ICR1 levels. LR developmental states were determined according to the work by Malamy and Benfey (41). (Scale bars: 50 μm.)

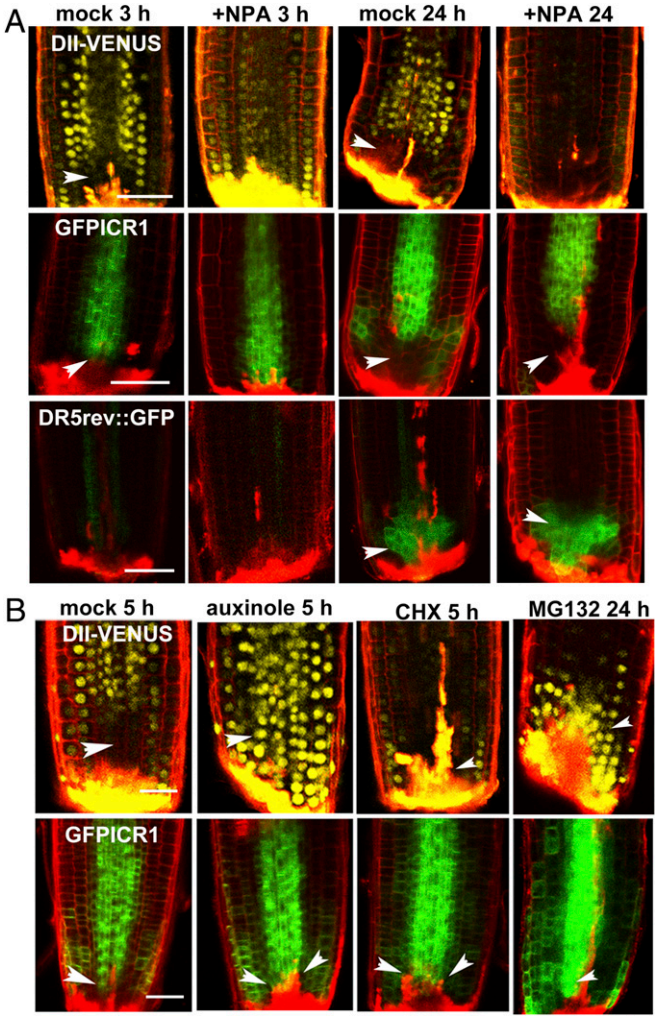

Fig. 4. GFP-ICR1 decay during root regeneration requires polar auxin transport, auxin-induced gene expression, de novo protein synthesis, and proteasome activity. (*A*) NPA inhibited GFP-ICR1 decay. DII-VENUS, $DR5_{rev}$::GFP, and GFP-ICR1 show the changes in auxin response and ICR1 stability in sectioned roots treated with the auxin transport inhibitor NPA. (*B*) DII-VENUS and GFP-ICR1 levels in sectioned root tips in the control and after incubation in the $SCF^{(TIR1/AFB)}$ inhibitor auxinole, the protein translation inhibitor CHX, and the proteasome inhibitor MG132. Arrowheads highlight the sites of auxin accumulation and GFP-ICR1 decay. (Scale bars: 50 μm.)

incubated with 10 μM protein translation inhibitor cycloheximide (CHX). After 5 h of incubation, the DII-VENUS signal was weaker compared with control mock treatments (Fig. 4*B*), presumably because CHX inhibited the replenishing of the DII-VENUS pool. However, the GFP-ICR1 signal did not decay from the sectioned root tips (Fig. 4*B*, GFPICR1 in the CHX 5 h column), strongly suggesting that the $SCF^{(TIR1/AFB)}$-mediated destabilization of ICR1 occurs through gene expression.

Treatments of roots with the proteasome inhibitor MG132 inhibited the decay of GFP-ICR1 (Fig. 4*B*, MG132 24 h), indicating that the absence of ICR1 at the root tip is proteasome-dependent. As expected (35), DII-VENUS was also stabilized by the MG132 treatment. From our data, we cannot conclude whether the inhibition of GFP-ICR1 decay by MG132 resulted from inhibition of auxin-dependent gene expression or direct involvement of the proteasome in ICR1 degradation. To conclude, the results in Figs. 2, 3, and 4 and Figs. S1–S4 established that ICR1 decay depends on auxin accumulation and $SCF^{(TIR1/AFB)}$-dependent gene expression.

It remained to be established whether GFP-ICR1 decay in non-meristematic cells also requires auxin-induced gene expression. To this end, seedlings were treated with 2,4-D. After 3 h of incubation with 2,4-D, the DII-VENUS signal was not detectable, whereas the $DR5_{rev}$::GFP signal started to appear in cells located ~500 μm shootward from the root tip (Fig. S3). Concomitantly, the GFP-ICR1 signal decayed. After 24 h of incubation with 2,4-D, the GFP-ICR1 signal further decayed. CHX treatments did not inhibit the decay of DII-VENUS but inhibited the increase of the *$DR5_{rev}$*::GFP signal and GFP-ICR1 decay. Hence, ICR1 stability depends on auxin-induced gene expression and de novo protein synthesis. Taken together, the data in Fig. S3 reconfirmed that ICR1 stability depends on cellular auxin levels and auxin-induced gene expression.

Asymmetric Destabilization of GFP-ICR After Gravitropic Stimuli. Auxin levels change rapidly in response to gravitropic stimuli, leading to its asymmetric distribution within minutes (36) (Fig. S5*B*). Reduced levels of GFP-ICR1 were observed in the upper side of gravitropic-stimulated roots as soon as 10 min after 90° root tilting (Fig. 5). The GFP-ICR1 signal continued to decay up to 20 min after gravitropic stimulation and in turn, gradually increased to its original level (Fig. 5). Similar to the root tip sectioning experiments, auxinole treatments inhibited the GFP-ICR1 and DII-VENUS signal decay (Fig. S5), indicating that GFP-ICR1 stability during gravitropic response also depended on auxin-induced gene expression. It has been shown that, in the upper side of a gravitropic-stimulated root tip, PIN2 is targeted to the vacuole and degraded in an $SCF^{(TIR1/AFB)}$-dependent mechanism (48–51). However, the degradation of PIN2 was observed only after 90 min of gravistimulation, and its levels reached a minimum after 4 h (48, 51). Hence, the decay of GFP-ICR1 coincides with the rapid change in auxin levels and likely precedes the degradation of PIN2.

The primary roots of the *icr1* mutant plants arrest soon after germination, preventing examination of their gravitropic response. However, the *icr1* mutant plants develop many adventitious roots, and some of them reach a length of 1–3 cm. These adventitious roots are agravitropic (27). The agravitropic phenotype of *icr1* adventitious roots and the countercorrelation between ICR1 and auxin levels suggest that regulation of ICR1 stability is critical for asymmetric auxin distribution after gravitropic stimuli. The transient destabilization of ICR1 may facilitate auxin accumulation at the lower side of gravitropic-stimulated roots, and at the same time, it may prevent formation of a new stable auxin maximum and enable auxin redistribution after the roots have reached the critical tipping point (36). It has yet to be discovered how gravitropic stimulus induces decay of GFP-ICR1 in the Lateral Root Cap (LRC) and epidermis.

Expression Pattern of ICR1 in Cotyledon and Leaves. Previously, we found that adaxial leaf epidermis pavement cells are deformed and that leaf vasculature is reduced in *icr1* (26, 27), suggesting a role for ICR1 in regulation of auxin transport in the areal organs of the plant. We recorded the expression patterns of GFP-ICR1 during cotyledon development and in mature leaves to examine whether the correlation between ICR1 expression and its function can be extended to other parts of the plant in addition to the root.

Single optical scans were used to determine the expression pattern of GFP-ICR1 in cotyledons and leaves at different developmental stages (Fig. S6 *A–H*). In torpedo (Fig. S6*A*) and mature embryos (Fig. S6 *B* and *C*), GFP-ICR1 was detected throughout the embryonic cotyledon protoderm. Higher expression levels were observed in the provascular tissues and the cotyledon tips (Fig. S6 *A*, arrowhead and *B*, arrowheads). In maturing cotyledon tips, 4 d after germination, GFP-ICR1 expression was high at the tip and the subtending provascular tissue (Fig. S6*D*). Strong GFP-ICR1 expression can be seen in a leaf primordium (Fig. S6*E*, arrowhead). A similar expression pattern in the cotyledon tip and provascular tissues of the embryo has previously been reported for the auxin

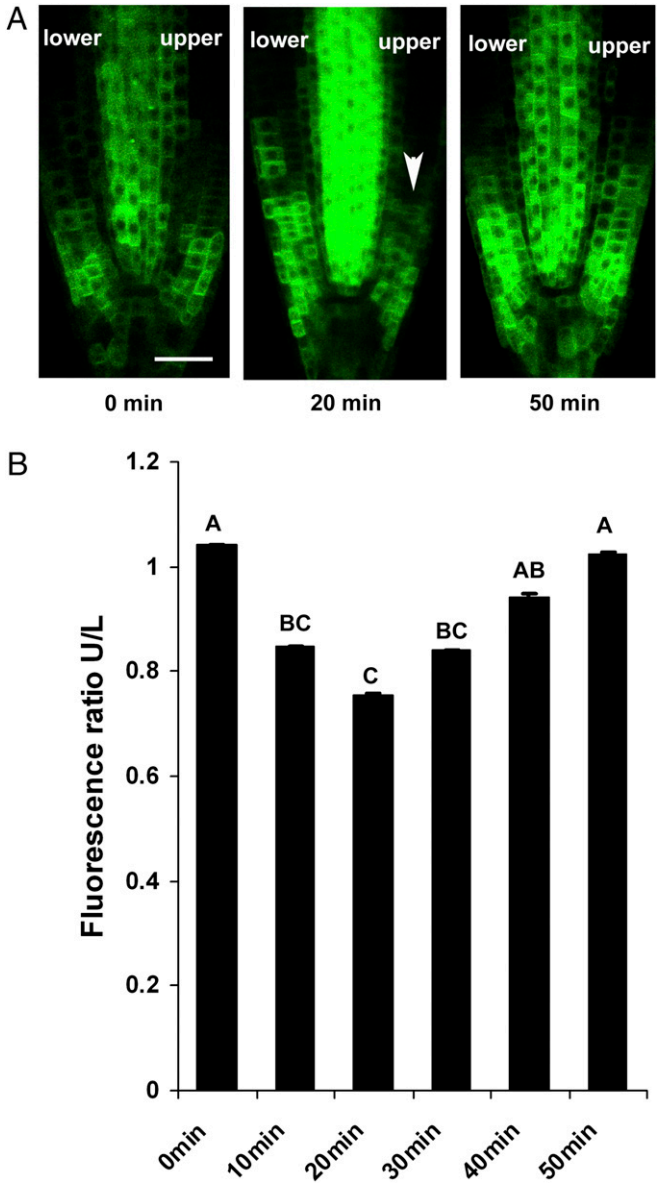

Fig. 5. GFP-ICR1 decay during gravitropic response. (*A*) Shortly after 90° tilting, GFP-ICR1 levels transiently decrease in the upper side (arrowhead). (*B*) Quantification of GFP-ICR1 levels in the upper and lower sides of 90°-tilted root tips. Letters above the bars designate statistically significant variance ($P \leq 0.01$ Tukey Kramer ANOVA). Error bars represent SE. (Scale bars: 50 μm.)

response reporter $DR5_{rev}$::GFP (5). It was further shown that the pattern of auxin distribution in the embryo is primarily because of PIN1 and PIN4 function rather than auxin biosynthesis (52).

A closer view of GFP-ICR1 expression in the epidermis during cotyledon maturation revealed a gradual decay of ICR1 expression in the epidermis. Two days after germination, GFP-ICR1 was detected throughout the epidermis (Fig. S6*F*). However, 5 days after germination, the GFP-ICR1 signal started to decay in maturing pavement cells and stomata (Fig. S6*G*, asterisks) while remaining high in dividing meristemoids. In a mature leaf (rosette leaf number 10 taken from a 6-wk-old plant), GFP-ICR1 expression was detected in dividing stomata lineage cells and absent from mature stomata guard and pavement cells (Fig. S6*H*). It has recently been shown that polar auxin transport and gradients regulate stomata development and patterning (53). The work by Le et al. (53) showed that, similar to GFP-ICR1, *PIN3* promoter-driven PIN3-GFP levels were high in meristemoids and guard mother cells and decreased in mature guard cells. Le et al. (53) also showed that stomata patterning was compromised in auxin transport and signaling mutants. Similarly, we also observed compromised stomata patterning in *icr1* (Fig. S6 *I* and *J*).

Taken together, the results shown in Fig. S6 indicate that, similar to the root, in aerial organs of *Arabidopsis*, there is a close correlation between ICR1 function in auxin transport and its expression pattern. The increase in GFP-ICR1 levels in the cotyledon tip and meristemoids, which corresponds to higher auxin response, resembles the increase in GFP-ICR1 levels in LR primordia (Fig. 3 and Fig. S4). The reduction in GFP-ICR1 in maturing cotyledon and leaf epidermis likely resulted from reduced auxin levels. Our observations indicate that the auxin-dependent posttranscriptional decay of GFP-ICR1 is specific to the root meristem.

Simulation of the Auxin–ICR1 Regulatory Feedback Loop. We developed a mathematical model describing ICR1-dependent auxin distribution in the root. Although various previous models have described PIN and AUX/Like AUX1 families regulated by auxin distribution in the root (6, 19, 22, 24, 54–58), we tried to examine a simpler model and see if it could explain some of the observed auxin distribution using the ICR1–auxin interactions. Our model assumes only that ICR1-dependent auxin transport polarizes to the opposite side from where auxin enters and that there is a nonmonotonic ICR1-dependent regulation of auxin transport according to auxin efflux rates. For the sake of simplicity, the ICR1-dependent auxin transport was depicted as a single entity, and auxin-dependent patterning and developmental processes were not taken into account. Our model consists of an $m \times n$ grid of cells. Each cell, uniquely identified by its location on the grid (i,j), is described by five differential equations: one equation describes the change in the amount of auxin in the cell $(AUX_{i,j})$ with respect to time, and four equations describe the change in the level of ICR1-dependent auxin transport in a cell's four-membrane planes ($ICR1_{i,j}^{Up}$, $ICR1_{i,j}^{Right}$, $ICR1_{i,j}^{Down}$, and $ICR1_{i,j}^{Left}$) with time. Given that the main sources of auxin during embryogenesis and plant growth are the embryo and the shoot (10, 59), auxin is assumed to enter the system through the upper row of cells $[(1,2),\ldots(1,n-1)]$ and be transported in both ICR1-dependent and -independent ways between adjacent cells. Auxin can be transported in all directions. The magnitude of auxin efflux in each direction is determined by the level of ICR1-mediated transport through a given membrane plane, the level of ICR1-independent transport in the system, and the overall auxin levels in the cell. For instance, the ICR1-dependent auxin efflux in the bottom membrane plane of cell (i,j) is proportional to $ICR1_{i,j}^{Down} \times AUX_{i,j}$. In turn, $ICR1_{i,j}^{Down}$ is affected by $ICR1_{i-1,j}^{Down} \times AUX_{i-1,j}$, which is the amount of auxin transported through the bottom membrane plane of the cell above cell (i,j). The lateral and shootward ICR1-dependent transports are modeled similarly, allowing auxin to be actively transported in all directions with no a priori constraints. ICR1 synthesis and degradation increase with auxin influx, with three relevant thresholds: one for ICR1-increased synthesis, one for saturation, and one for ICR1 degradation (similar to PIN regulation described in refs. 55 and 56). A detailed graphical explanation of the model components and parameters are presented in Fig. S7 and Table S2.

Our mathematical model supports the assumption that ICR1-regulated polar auxin transport is sufficient for generating the auxin distribution observed in root tips without requiring any specific assumption regarding auxin transporters. Our system has reached a stable state similar to the experimental results: high auxin concentration near the root tip and canalization (Fig. 6*A*) as well as a "reverse-fountain" pattern (60), with auxin reflux through the outermost cell columns (Fig. 6*A*). The corresponding ICR1

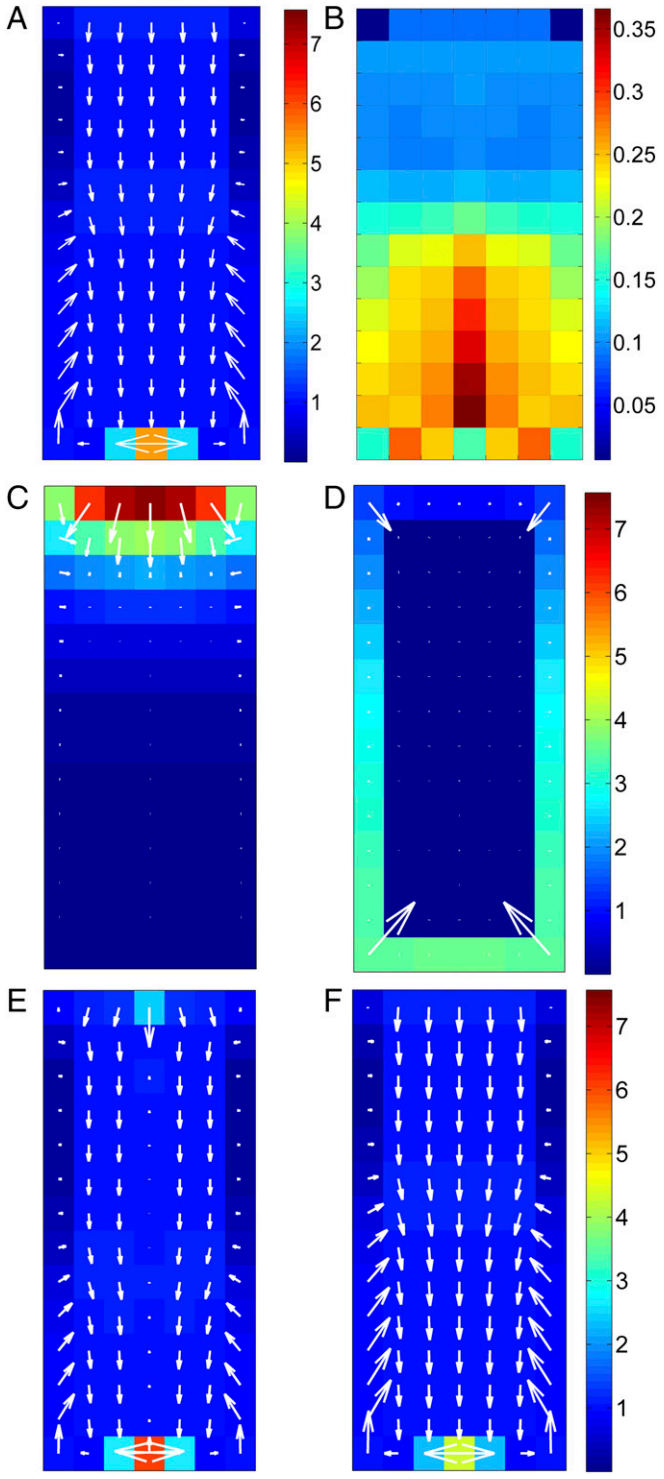

Fig. 6. Simulation of ICR1-dependent auxin distribution. (*A*) WT root. The system reaches a steady state, where auxin maximum is obtained near the root tip when assuming that ICR1 is involved in directional auxin transport. (*B*) ICR1 distribution in WT root at a steady state. The system did not stabilize in the case of (*C*) absence of ICR1-mediated auxin transport or (*D*) low ICR1 degradation rate. (*E*) Simulation of auxin maximum regeneration after root sectioning. The bottom rows of a root at equilibrium (where the auxin maximum is formed) were removed and replaced with rows from the middle of the root in terms of auxin and ICR1 values. The system reached a stable steady state in terms of auxin distribution and fluxes similar to untreated root. Arrows denote the direction of the auxin flow. (*F*) Auxin distribution with auxin synthesis at the root tip. The model was simulated to (*A*) the stable state, and then, an auxin biosynthesis term (*AuxSynth* = 0.001) was added to cells with high auxin concentrations (*Auxin* > 1). The system reached (*A*) a stable state similar to that reached without auxin biosynthesis, maintaining a similar auxin flow patterns as well.

pattern is also consistent with the observed ICR1 canalization and a local ICR1 minimum at the location of the auxin maximum (Fig. 6*B*). We further examined our model under several additional scenarios. First, we assumed no active transport of auxin, which resulted in a gradual decrease of auxin toward the root tip (Fig. 6*C*) and is consistent with the dissipation of the auxin maximum in *icr1* mutant root tips (26, 27). Second, we studied the effect of a slower ICR1 degradation rate. This condition resulted in reduction of the auxin maximum at the root tip and a rapid appearance of high auxin maxima at the outer layers of the top of the root (Fig. 6*D*). This scenario is consistent with the dissipation of the auxin maximum and the formation of adventitious roots observed in *pCMI2>>GFP-ICR1* plants (Fig. 1*F*). Third, we simulated root sectioning by removing the bottom rows of a root at equilibrium—the ones containing the auxin maximum—and replacing them by typical rows in terms of auxin and ICR1 values chosen from the middle of the root. The system resumed to a similar pattern with qualitatively identical auxin distribution (Fig. 6*E*). Fourth, similar to the results shown in Fig. 6*A*, local auxin maximum formed at the bottom of the grid when the simulation was run assuming a low level of auxin synthesis at the site of formation of the future auxin maximum (Fig. 6*F*).

The assumption made in our model that the ICR1-dependent auxin transport polarizes to the opposite side from where auxin enters is consistent with experimental data and modeling, which showed that PIN-dependent auxin transport polarizes away from the site of auxin synthesis (58, 59). The linkage between cellular auxin levels, ICR1 stability, and auxin distribution is also consistent with a recently described model, which showed that asymmetric auxin distribution at the root tip results from PIN-dependent directional auxin transport and cellular auxin levels (19). Previous works modeled the auxin distribution assuming an auxin sink, a specific spatial distribution of auxin transporters, or a dependency on auxin gradient and/or flux (20, 22, 24, 61). Differently, we assume a nonmonotonic relationship between the auxin flux and ICR1 levels, which allows auxin to be concentrated at the root tip and create the backflow pattern.

Our experimental work and modeling imply that the cellular levels of ICR1 are subject to dual regulation by auxin. ICR1 expression is induced as auxin concentrations increase and destabilized rapidly in a cell-specific manner when auxin intracellular concentrations exceed a critical level. Our work further suggests that the function of ICR1 in recruitment of PINs to the plasma membrane (26) together with the bimodal regulation of its levels by auxin (this work) could be involved in regulating directional auxin transport, canalization, formation of a local auxin maximum, and shootward reflux in the root epidermis. Hence, ICR1 could be part of an auxin-dependent self-organizing mechanism. Additional work will be required to elucidate how ICR1 regulates PIN distribution and its integration with ROP and possibly, other signaling networks in the cell.

Materials and Methods

Plant Material and Treatments. All transgenic plants are in the *Columbia-0* background. Plants used in this study were *DII-VENUS* (35), *DR5*$_{rev}$*::GFP* (5), *pICR1>>GFP-ICR1* (26), *35S::GFP-ICR1* (27), *pICR1>>ICR1-mCherry*, and *pCMI2>>GFP-ICR1* (this study). Plants were grown as previously described (26). Root tip sectioning was carried out as previously described (34). Gravitropic stimuli were induced by a 90° tilting of vertically grown seedling for the indicated time. Quantification of GFP-ICR1 and DII-VENUS levels was carried out on about 10–30 seedlings for each time point.

Chemical Treatments. Stock solutions were prepared as follows: IAA (Sigma) and NAA (Sigma) in ethanol, 2,4-D (Sigma) in 0.1 M KOH in ethanol, and NPA (Duchefa), MG132 (Calbiochem), CHX (Sigma), and auxinole (a gift from Ken-ichiro Hayashi, Okayama University of Science, Okayama, Japan) (46, 47) in DMSO. Dilution into medium was at indicated concentrations.

Microscopy. Images were obtained with an SV-11 stereomicroscope (Zeiss), Axioplan 2 Imaging microscope (Zeiss), TSC-SL laser-scanning confocal microscope (Leica), and LSM-780-NLO combined laser-scanning confocal microscope and multiphoton microscope (Zeiss). Image analysis was carried out with Leica TCS, Zeiss Zen10, Fiji (Image J), and Adobe Photoshop 6. Each experiment was repeated at least three times.

Mathematical Model. We constructed an $m \times n$ array of cells modeling a root tip. In each cell (i,j), we modeled the auxin concentration $(AUX_{i,j})$ and the level of ICR1-dependent auxin efflux through the four membrane planes $(ICR1^{Up}_{i,j}, ICR1^{Right}_{i,j}, ICR1^{Down}_{i,j}$, and $ICR1^{Left}_{i,j})$ of each cell. Full experimental procedures, details of the mathematical model, and associated references are available in *SI Materials and Methods*.

ACKNOWLEDGMENTS. We thank K. Hayashi for sharing published materials, the Manna Center for Plant Biology at Tel Aviv University for support, and S. McCormick for critical reading of the manuscript. This research was supported by Israel Science Foundation Grants 1568/13 (to L.H.), 1244/11 (to S.Y.), and 1125/13 (to S.Y.) and US–Israel Binational Science Foundation Grant BSF 2009309 (to S.Y.).

1. Uggla C, Moritz T, Sandberg G, Sundberg B (1996) Auxin as a positional signal in pattern formation in plants. *Proc Natl Acad Sci USA* 93(17):9282–9286.
2. Sabatini S, et al. (1999) An auxin-dependent distal organizer of pattern and polarity in the Arabidopsis root. *Cell* 99(5):463–472.
3. Reinhardt D, et al. (2003) Regulation of phyllotaxis by polar auxin transport. *Nature* 426(6964):255–260.
4. Benková E, et al. (2003) Local, efflux-dependent auxin gradients as a common module for plant organ formation. *Cell* 115(5):591–602.
5. Friml J, et al. (2003) Efflux-dependent auxin gradients establish the apical-basal axis of Arabidopsis. *Nature* 426(6963):147–153.
6. Grieneisen VA, Xu J, Marée AF, Hogeweg P, Scheres B (2007) Auxin transport is sufficient to generate a maximum and gradient guiding root growth. *Nature* 449(7165):1008–1013.
7. Vanneste S, Friml J (2009) Auxin: A trigger for change in plant development. *Cell* 136(6):1005–1016.
8. Leyser O (2011) Auxin, self-organisation, and the colonial nature of plants. *Curr Biol* 21(9):R331–R337.
9. Abley K, et al. (2013) An intracellular partitioning-based framework for tissue cell polarity in plants and animals. *Development* 140(10):2061–2074.
10. Ljung K, Bhalerao RP, Sandberg G (2001) Sites and homeostatic control of auxin biosynthesis in Arabidopsis during vegetative growth. *Plant J* 28(4):465–474.
11. Ljung K, et al. (2005) Sites and regulation of auxin biosynthesis in Arabidopsis roots. *Plant Cell* 17(4):1090–1104.
12. Gälweiler L, et al. (1998) Regulation of polar auxin transport by AtPIN1 in Arabidopsis vascular tissue. *Science* 282(5397):2226–2230.
13. Wisniewska J, et al. (2006) Polar PIN localization directs auxin flow in plants. *Science* 312(5775):883.
14. Barbosa IC, Schwechheimer C (2014) Dynamic control of auxin transport-dependent growth by AGCVIII protein kinases. *Curr Opin Plant Biol* 22C:108–115.
15. Barbosa IC, Zourelidou M, Willige BC, Weller B, Schwechheimer C (2014) D6 PROTEIN KINASE activates auxin transport-dependent growth and PIN-FORMED phosphorylation at the plasma membrane. *Dev Cell* 29(6):674–685.
16. Zourelidou M, et al. (2014) Auxin efflux by PIN-FORMED proteins is activated by two different protein kinases, D6 PROTEIN KINASE and PINOID. *eLife* 3:02860.
17. Swarup R, et al. (2001) Localization of the auxin permease AUX1 suggests two functionally distinct hormone transport pathways operate in the Arabidopsis root apex. *Genes Dev* 15(20):2648–2653.
18. Stepanova AN, et al. (2008) TAA1-mediated auxin biosynthesis is essential for hormone crosstalk and plant development. *Cell* 133(1):177–191.
19. Band LR, et al. (2014) Systems analysis of auxin transport in the Arabidopsis root apex. *Plant Cell* 26(3):862–875.
20. Mitchison GJ (1981) The polar transport of auxin and vein patterns in plants. *Philos Trans R Soc Lond B Biol Sci* 295(1078):461–471.
21. Sachs T (1981) The control of the pattern differentiation of vascular tissue. *Adv Bot Res* 9:151–162.
22. Krupinski P, Jönsson H (2010) Modeling auxin-regulated development. *Cold Spring Harb Perspect Biol* 2(2):a001560.
23. Sauer M, et al. (2006) Canalization of auxin flow by Aux/IAA-ARF-dependent feedback regulation of PIN polarity. *Genes Dev* 20(20):2902–2911.
24. Wabnik K, Govaerts W, Friml J, Kleine-Vehn J (2011) Feedback models for polarized auxin transport: An emerging trend. *Mol Biosyst* 7(8):2352–2359.
25. Furutani M, Nakano Y, Tasaka M (2014) MAB4-induced auxin sink generates local auxin gradients in Arabidopsis organ formation. *Proc Natl Acad Sci USA* 111(3):1198–1203.
26. Hazak O, et al. (2010) A rho scaffold integrates the secretory system with feedback mechanisms in regulation of auxin distribution. *PLoS Biol* 8(1):e1000282.
27. Lavy M, et al. (2007) A Novel ROP/RAC effector links cell polarity, root-meristem maintenance, and vesicle trafficking. *Curr Biol* 17(11):947–952.
28. Moore I, Gälweiler L, Grosskopf D, Schell J, Palme K (1998) A transcription activation system for regulated gene expression in transgenic plants. *Proc Natl Acad Sci USA* 95(1):376–381.
29. Poraty-Gavra L, et al. (2013) The Arabidopsis Rho of plants GTPase AtROP6 functions in developmental and pathogen response pathways. *Plant Physiol* 161(3):1172–1188.
30. Hruz T, et al. (2008) Genevestigator V3: A reference expression database for the meta-analysis of transcriptomes. *Adv Bioinformatics* 2008(2008):420747.
31. Friml J, et al. (2002) AtPIN4 mediates sink-driven auxin gradients and root patterning in Arabidopsis. *Cell* 108(5):661–673.
32. Blilou I, et al. (2005) The PIN auxin efflux facilitator network controls growth and patterning in Arabidopsis roots. *Nature* 433(7021):39–44.
33. Vieten A, et al. (2005) Functional redundancy of PIN proteins is accompanied by auxin-dependent cross-regulation of PIN expression. *Development* 132(20):4521–4531.
34. Sena G, Wang X, Liu HY, Hofhuis H, Birnbaum KD (2009) Organ regeneration does not require a functional stem cell niche in plants. *Nature* 457(7233):1150–1153.
35. Brunoud G, et al. (2012) A novel sensor to map auxin response and distribution at high spatio-temporal resolution. *Nature* 482(7383):103–106.
36. Band LR, et al. (2012) Root gravitropism is regulated by a transient lateral auxin gradient controlled by a tipping-point mechanism. *Proc Natl Acad Sci USA* 109(12):4668–4673.
37. Hosek P, et al. (2012) Auxin transport at cellular level: New insights supported by mathematical modelling. *J Exp Bot* 63(10):3815–3827.
38. Kramer EM, Bennett MJ (2006) Auxin transport: A field in flux. *Trends Plant Sci* 11(8):382–386.
39. Petrásek J, et al. (2006) PIN proteins perform a rate-limiting function in cellular auxin efflux. *Science* 312(5775):914–918.
40. Swarup K, et al. (2008) The auxin influx carrier LAX3 promotes lateral root emergence. *Nat Cell Biol* 10(8):946–954.
41. Malamy JE, Benfey PN (1997) Organization and cell differentiation in lateral roots of Arabidopsis thaliana. *Development* 124(1):33–44.
42. Haecker A, et al. (2004) Expression dynamics of WOX genes mark cell fate decisions during early embryonic patterning in Arabidopsis thaliana. *Development* 131(3):657–668.
43. Rademacher EH, et al. (2012) Different auxin response machineries control distinct cell fates in the early plant embryo. *Dev Cell* 22(1):211–222.
44. Wendrich JR, Weijers D (2013) The Arabidopsis embryo as a miniature morphogenesis model. *New Phytol* 199(1):14–25.
45. Casimiro I, et al. (2001) Auxin transport promotes Arabidopsis lateral root initiation. *Plant Cell* 13(4):843–852.
46. Hayashi K, et al. (2012) Rational design of an auxin antagonist of the SCF(TIR1) auxin receptor complex. *ACS Chem Biol* 7(3):590–598.
47. Hayashi K, et al. (2008) Small-molecule agonists and antagonists of F-box protein-substrate interactions in auxin perception and signaling. *Proc Natl Acad Sci USA* 105(14):5632–5637.
48. Abas L, et al. (2006) Intracellular trafficking and proteolysis of the Arabidopsis auxin-efflux facilitator PIN2 are involved in root gravitropism. *Nat Cell Biol* 8(3):249–256.
49. Kleine-Vehn J, et al. (2008) Differential degradation of PIN2 auxin efflux carrier by retromer-dependent vacuolar targeting. *Proc Natl Acad Sci USA* 105(46):17812–17817.
50. Leitner J, et al. (2012) Lysine63-linked ubiquitylation of PIN2 auxin carrier protein governs hormonally controlled adaptation of Arabidopsis root growth. *Proc Natl Acad Sci USA* 109(21):8322–8327.
51. Baster P, et al. (2013) SCF(TIR1/AFB)-auxin signalling regulates PIN vacuolar trafficking and auxin fluxes during root gravitropism. *EMBO J* 32(2):260–274.
52. Weijers D, et al. (2005) Maintenance of embryonic auxin distribution for apical-basal patterning by PIN-FORMED-dependent auxin transport in Arabidopsis. *Plant Cell* 17(9):2517–2526.
53. Le J, et al. (2014) Auxin transport and activity regulate stomatal patterning and development. *Nat Commun* 5:3090.
54. Kramer EM (2004) PIN and AUX/LAX proteins: Their role in auxin accumulation. *Trends Plant Sci* 9(12):578–582.
55. Mironova VV, et al. (2012) Combined in silico/in vivo analysis of mechanisms providing for root apical meristem self-organization and maintenance. *Ann Bot (Lond)* 110(2):349–360.
56. Mironova VV, et al. (2010) A plausible mechanism for auxin patterning along the developing root. *BMC Syst Biol* 4:98.
57. van Berkel K, de Boer RJ, Scheres B, ten Tusscher K (2013) Polar auxin transport: Models and mechanisms. *Development* 140(11):2253–2268.
58. Wabnik K, Robert HS, Smith RS, Friml J (2013) Modeling framework for the establishment of the apical-basal embryonic axis in plants. *Curr Biol* 23(24):2513–2518.
59. Robert HS, et al. (2013) Local auxin sources orient the apical-basal axis in Arabidopsis embryos. *Curr Biol* 23(24):2506–2512.
60. Kleine-Vehn J, Friml J (2008) Polar targeting and endocytic recycling in auxin-dependent plant development. *Annu Rev Cell Dev Biol* 24:447–473.
61. Stoma S, et al. (2008) Flux-based transport enhancement as a plausible unifying mechanism for auxin transport in meristem development. *PLOS Comput Biol* 4(10):e1000207.